The Journal of Neuroscience, March 1990, 10(3): 795–813

Three-Dimensional Autoradiographic Localization of Quench-Corrected Glycine Receptor Specific Activity in the Mouse Brain Using ^{3}H-Strychnine as the Ligand

W. Frost White,[1,a] Steven O'Gorman,[2] and Anna W. Roe[1,b]

[1]Department of Neuroscience, Children's Hospital, and Harvard Medical School, Boston, Massachusetts 02115, and [2]Department of Developmental Neurobiology, Salk Institute, La Jolla, California 92037

The autoradiographic analysis of neurotransmitter receptor distribution is a powerful technique that provides extensive information on the localization of neurotransmitter systems. Computer methodologies are described for the analysis of autoradiographic material which include quench correction, 3-dimensional display, and quantification based on anatomical boundaries determined from the tissue sections. These methodologies are applied to the problem of the distribution of glycine receptors measured by ^{3}H-strychnine binding in the mouse CNS. The most distinctive feature of this distribution is its marked caudorostral gradient. The highest densities of binding sites within this gradient were seen in somatic motor and sensory areas; high densities of binding were seen in branchial efferent and special sensory areas. Moderate levels were seen in nuclei related to visceral function. Densities within the reticular formation paralleled the overall gradient with high to moderate levels of binding. The colliculi had low and the diencephalon had very low levels of binding. No binding was seen in the cerebellum or the telencephalon with the exception of the amygdala, which had very low levels of specific binding. This distribution of glycine receptors correlates well with the known functional distribution of glycine synaptic function. These data are illustrated in 3 dimensions and discussed in terms of the significance of the analysis techniques on this type of data as well as the functional significance of the distribution of glycine receptors.

GABA and glycine are the major inhibitory neurotransmitters in the mammalian CNS. GABA-mediated inhibition is found throughout the neuraxis but is most prominent in rostral brain areas. On the other hand, glycine mediated inhibition appears to be limited to posterior brain regions (Aprison and Nadi, 1977). A greater understanding of the distribution of GABA and glycine neurotransmitter function and the relationship between GABA and glycine-mediated inhibition would clarify the regional specificity of inhibition mediated by these 2 neurotransmitters and further define their functional interrelationships. In this paper we present data on the distribution of inhibitory postsynaptic glycine receptors in the mouse CNS.

The anatomical localization of neurotransmitter receptors provides detailed information on the distribution of the postsynaptic response potential of different regions to neurotransmitter activation. Combined with similar data on presynaptic function, this information defines the functional anatomy of neurotransmitter systems and thus is an important aspect of the biochemical anatomy of the nervous system. Receptor localization in experimental material increases our understanding of the consequences of manipulations; similar studies on pathological material may shed light on the causes and consequences of disease states (Whitehouse, 1985; Palacios et al., 1986).

Studies on the localization of neurotransmitter receptors have been greatly facilitated by the development of specific binding assays for slide-mounted tissue sections combined with reliable diffusable substance autoradiographic techniques (Young and Kuhar, 1979; Kuhar, 1985). Numerous studies employing these techniques have defined the anatomical localization of most known neurotransmitter receptors in a variety of mammalian and nonmammalian species (Kuhar, 1985; Kuhar et al., 1986; Palacios et al., 1986). The application of computer-assisted analysis methodologies has greatly facilitated the quantification and interpretation of autoradiographic data (Goochee et al., 1980; Palacios et al., 1981; Altar et al., 1984; Hibbard and Hawkins, 1984; Stein et al., 1984; Davis et al., 1986; Zilles et al., 1986).

There are 2 significant limitations with current methodologies for receptor quantitation. The first is differential efficiency of tritiated ligands in exposing silver grains depending on the tissue localization of the ligand (Alexander et al., 1981; Herkenham and Sokoloff, 1984; Geary and Wooten, 1985; Kuhar and Unnerstall, 1985). The second is inadequate quantitation of receptor-specific activity in individual sections through 3-dimensional morphological regions. In this paper we address these limitations using computer methodologies and present the quench corrected 3-dimensional distribution of glycine receptors in the mouse central nervous system using ^{3}H-strychnine as the ligand.

Materials and Methods

Six adult male C57BL/6J mice were used in this study. The mice were bred and raised in the animal facilities at Children's Hospital, Boston.

Received Feb. 3, 1989; revised Aug. 2, 1989; accepted Sept. 11, 1989.

We thank the members of the Image Graphics Lab at Children's Hospital for their help in developing the software used in these studies. We are especially thankful to Josh Simons, Linda Kirschner, Monty Brandenberg, Nariman Shimbayati, and Bob Pearlstein. This work was supported by NIH Grant NS20808 and the Children's Hospital Mental Retardation Core Grant HD06276.

Correspondence should be addressed to: Dr. W. Frost White, Department of Neuroscience, Pfizer Central Research, Pfizer, Inc., Eastern Point Road, Groton, CT 06340.

[a] Present address: Department of Neuroscience, Pfizer Central Research, Pfizer, Inc., Eastern Point Road, Groton, CT 06340,

[b] Present address: Department of Brain and Cognitive Science, Massachusetts Institute of Technology, Cambridge, MA 02139.

The data presented in this paper are from one representative animal. The same qualitative results were seen for all the animals.

The methods for ^{3}H-strychnine binding to slide-mounted tissue sections were similar to those reported for rat CNS (Zarbin et al., 1981) with several modifications that facilitated cutting the brain, improved specific binding, and decreased nonspecific binding. Mice were perfused intracardially with 250 ml of fixative solution consisting of 0.1% paraformaldehyde, 100 mM NaCl, 320 mM sucrose, 50 mM sodium phosphate buffer (pH 7.4), followed by 50 ml of the same solution without the paraformaldehyde. The brain and spinal cord to the cervical spinal cord level of C3 were rapidly removed and frozen onto a cryostat chuck with O.C.T. compound (Miles Scientific). Serial 10-μm sections were cut on a cryostat, mounted on gelatin-coated microscope slides, air-dried, and stored desiccated for up to 2 months at −20°C prior to use. Storage did not alter the results.

Sections separated by approximately 120 μm were preincubated for 1 hr in 100 mM NaCl, 50 mM sodium phosphate buffer (pH 7.4) to remove endogenous ligands, incubated 1 hr in 5 nM ^{3}H-strychnine in this buffer to label receptors, washed in 4 changes of fresh buffer for a total of 1 min to reduce nonspecific binding, dipped in distilled water to prevent salt crystal formation, and rapidly dried with anhydrous air to trap the ligand on or near the receptor. Adjacent sections were incubated in buffer containing ^{3}H-strychnine and 10 mM glycine to determine nonspecific binding. Autoradiograms were prepared by exposing the sections to LKB Ultrofilm-^{3}H for 4 weeks. Films were developed in Kodak D-19 for 5 min, stopped in H_2O for 15 sec, fixed in Kodak Rapid Fix for 5 min, and washed in H_2O for 1 hr, all at 19°C.

Differential efficiency was determined using the method of Herkenham and Sokoloff (1984). Following exposure, the same sections used for ^{3}H-strychnine binding studies were preincubated at room temperature in 3 changes of 100 mM NaCl, 50 mM Tris-HCl buffer (pH 7.2) at 22°C for a total of 4 hr. This resulted in complete dissociation of bound ^{3}H-strychnine as shown in parallel experiments. Sections were then incubated in 4 nM ^{3}H-succinimidyl propionate at 22°C for 30 min, followed by a 10-min wash in 4 changes of fresh buffer and 10 sec in distilled water. The sections were exposed to Ultrofilm-^{3}H for 10 d. Lipids were removed from a series of sections labeled with ^{3}H-succinimidyl propionate by first dehydrating in ascending alcohol concentrations, followed by 1 hr in xylene, and rehydrating in descending concentrations of alcohol (Herkenham and Sokoloff, 1984). The sections were then reexposed to Ultrofilm-^{3}H for 10 d. Adjacent sections were processed identically following incubation with 0.06 nM ^{125}I-Bolton and Hunter reagent to assess the labeling with a compound that has the same binding characteristics as succinimidyl propionate but does not show differential efficiency. Following exposure to the film, the sections were stained with cresyl violet for anatomical analyses.

Quantitative analyses were performed using software developed on a VAX 11-780 computer in the Image Graphics Laboratory at Children's Hospital, Boston. The density of exposed silver grains was digitized on an Optronics P-1000 scanning drum densitometer at a resolution of 50 μm. The average optical density of the film surrounding the exposed autoradiograms was subtracted from the optical density values of each pixel within the autoradiograms to correct for film background. Optical density was converted to specific activity using a cubic fit to the relationship between optical density (following the subtraction of film background) and specific activity from a step wedge standard (Amersham) and rat whole brain paste standards exposed with the experimental material. Following conversion to specific activity, each image was registered with an image from an adjacent section that had been processed for nonspecific binding and the nonspecific binding values were subtracted pixel by pixel. Receptor distribution maps were smoothed by a nearest-neighbor averaging routine to produce images with greater spatial contiguity. The smoothing algorithm employed was 2 pixels deep and weighted by the inverse square law. This algorithm was chosen because it produced adequate spatial contiguity of the autoradiographic distribution and maintained the spatial distribution of the image. The smoothed receptor distribution maps were used to draw isodensity contours which circumscribe areas of equivalent binding used in the registration and 3-dimensional display of the data. Additional filtering of the isodensity contours was performed to reduce the complexity of the resulting image. This was accomplished using a 4-point spline routine. Graphic images were displayed and registered on a Megatek 7295 3-D color raster display monitor. Photographs were taken either directly from the Megatek screen or with a Dunn camera.

The boundaries of anatomical nuclei were digitized from camera lucida drawings of the stained sections using a bitpad. Anatomical boundaries were determined according to Sidman et al. (1971), and Paxinos and Watson (1986). Registration with receptor distribution data was performed using algorithms developed for the raster display monitor. Nuclear boundary contours were compared with receptor distribution data and, if warranted, modified where there were obvious discrepancies. Conservative estimates of nuclear boundaries were used where ambiguities existed.

Materials. ^{3}H-Strychnine, 23 Ci/mmol, was purchased from New England Nuclear; ^{3}H-succinimidyl propionate, 80 Ci/mmol, and ^{125}I-Bolton and Hunter reagent, 2000 Ci/mmol, were purchased from Amersham. Ultrofilm-^{3}H was purchased from LKB. All other chemicals were from Sigma.

Results

Binding sites for ^{3}H-strychnine were confined to gray-matter areas in posterior regions of the mouse CNS with no significant binding observed in white-matter areas. Binding sites for ^{3}H-strychnine had a marked caudorostral distribution. The highest levels of specific binding were seen in the spinal cord and posterior brain stem. Lower levels were seen in the anterior brain stem and midbrain, and still lower levels in the diencephalon. No specific binding was seen in the telencephalon (with the exception of low levels of binding in the amygdala) or the cerebellum.

An example of a stained tissue section from the mouse brain stem and the resulting autoradiogram from LKB Ultrofilm-^{3}H is shown in Figure 1, *A, B*. Color-coded, digitized images of the distribution of ^{3}H-strychnine binding to the brain-stem section shown in Figure 1 are shown in the middle row of Figure 2. Figure 2*D* is the distribution displayed as optical density as digitized from the film record; Figure 2*E* is the distribution displayed as specific activity following the subtraction of film background. Nonspecific binding determined on adjacent sections incubated with ^{3}H-strychnine and 10 mM glycine was indistinguishable from film background; therefore, no further correction was required for nonspecific binding. Figure 2*F* is the distribution displayed as specific activity following nearest-neighbor smoothing to produce an image with greater spatial contiguity. At this level of the mouse brain stem, high levels of ^{3}H-strychnine binding sites were observed in the hypoglossal nucleus and the nucleus of the spinal tract of 5; no specific binding was seen in the cerebellum.

Ligands used for the localization of neurotransmitter receptors often are labeled with tritium because of the ease of labeling and purification, the high specific activity obtained, the stability, and the pharmacological similarity of the labeled compound to the parent compound (Bennett and Yamamura, 1985). The low energy of the beta emission produced by tritium has both advantages and disadvantages. The major advantage is that the path length is short, which results in a high degree of spatial resolution within the tissue section (Rogers, 1979). It also makes it possible to cut relatively thin sections that are infinitely thick in relation to path length; thus minor variations in section thickness do not produce variations in perceived receptor density (Falk and King, 1963; Caviness and Barkley, 1971; Alexander et al., 1981). The major disadvantage is the differential efficiency of bound tritiated ligands in exposing silver grains depending on the localization of the ligand in the tissue (Alexander et al., 1981; Herkenham and Sokoloff, 1984; Geary and Wooten, 1985; Kuhar and Unnerstall, 1985). The lipid content of the tissue contributes to the differential efficiency because the efficiency is lowest in areas of high lipid content, such as myelinated fiber

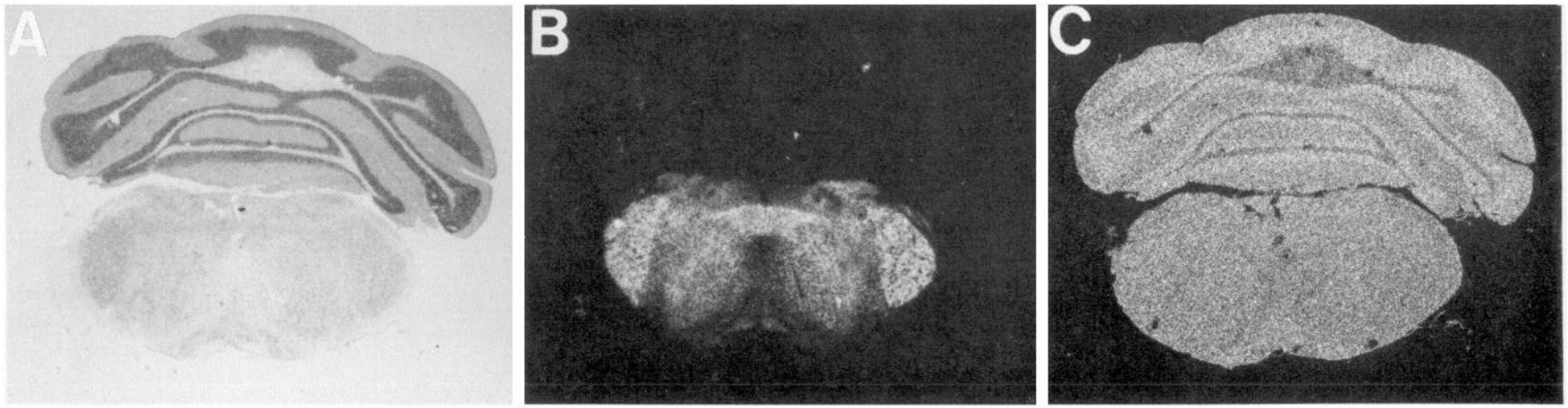

Figure 1. Representative cresyl-violet-stained section (*A*) and dark-field Ultrofilm-^{3}H autoradiograms following exposure to the same section incubated in ^{3}H-strychnine to localize glycine receptors (*B*) or ^{3}H-succinimidyl propionate to measure relative quench (*C*). The section was taken from the mid-brain-stem level of the mouse.

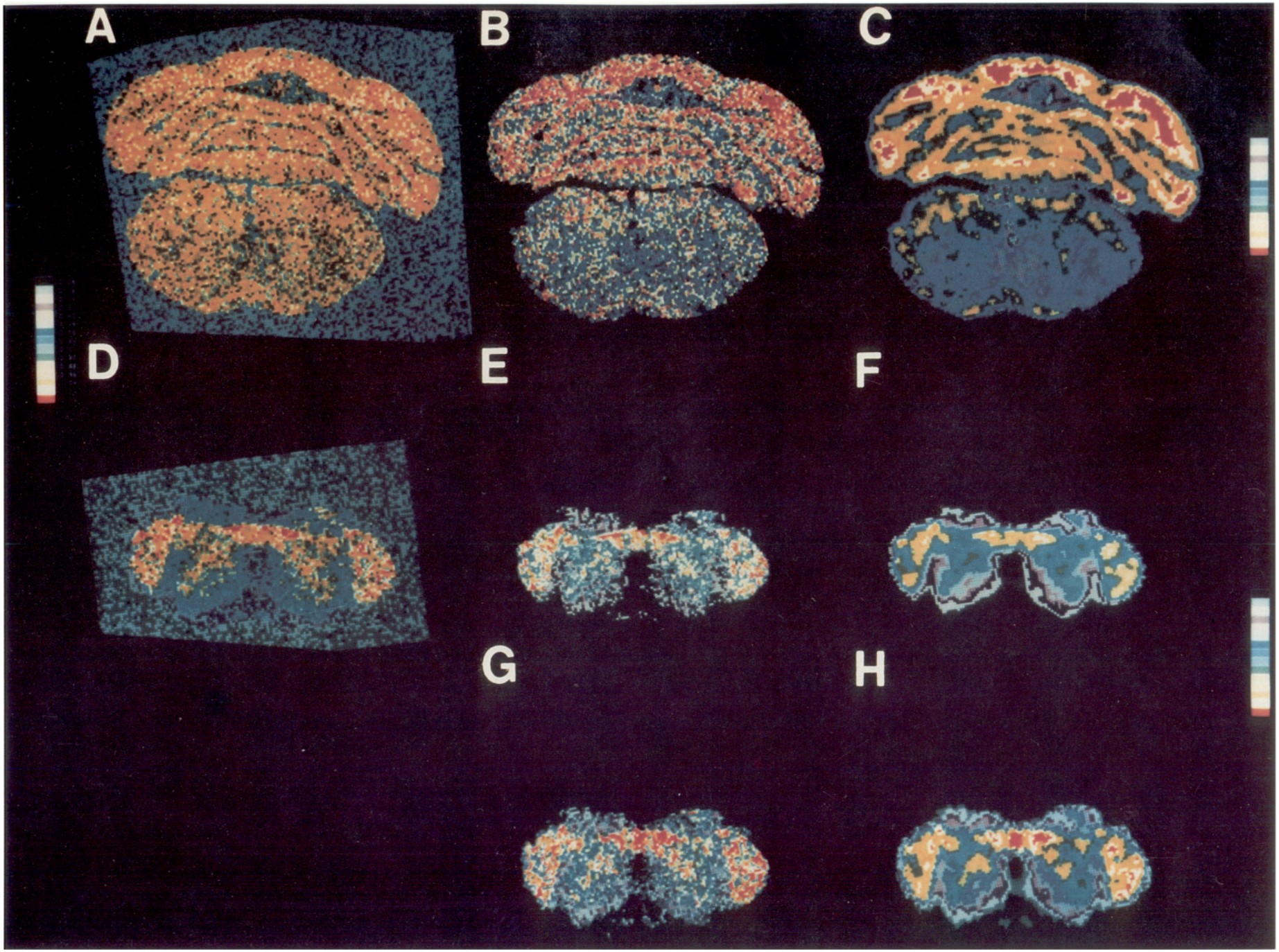
A
B
C
D
E
F
G
H

pathways, and delipidating the tissue with organic solvents removes differential efficiency (Herkenham and Sokoloff, 1984; Geary et al., 1985). Although procedures have been developed for removing differential efficiency by removing lipids in localization studies for several neurotransmitter receptors (Herkenham and Pert, 1982), this is not applicable to ligands for many receptors where the delipidating procedure also removes the bound ligand (Kuhar and Unnerstall, 1982).

A general method for correcting differential efficiency using computer methodologies was developed. This method relies on the uniform binding of ^{3}H-succinimidyl propionate to CNS tissue sections. The uniform labeling by ^{3}H-succinimidyl propionate has been shown by the uniform optical density of ^{3}H-succinimidyl propionate-labeled sections following lipid removal and the uniform autoradiographic density obtained from tissue sections labeled with ^{125}I-Bolton and Hunter reagent (Herkenham and Sokoloff, 1984; and this study, data not shown); ^{3}H-succinimidyl propionate is a tritiated analog of ^{125}I-Bolton and Hunter reagent and ^{125}I is not differentially quenched by tissue constituents.

The Ultrofilm-^{3}H autoradiogram for ^{3}H-succinimidyl propionate binding to the mouse brain section shown in Figure 1*A* is shown in Figure 1*C*. The top row of Figure 2 shows the color-coded, digitized distribution of (*A*) optical density, (*B*) specific activity, and (*C*) smoothed specific activity of ^{3}H-succinimidyl propionate binding to the same section shown for ^{3}H-strychnine binding in the middle row. Because ^{3}H-succinimidyl propionate binds uniformly to the tissue section, the differences in optical density and specific activity observed in these images resulted from differential efficiency due to tissue localization. The relative efficiency of the ^{3}H-succinimidyl propionate images was determined by comparing the specific activity of the images before and after delipidation. From these images it is apparent that the efficiency in the granule cell layers of the cerebellum and in dorsal nuclei of the brain stem was high (85 ± 11%) and the efficiency in the white-matter areas of both cerebellum and brain stem was low (39 ± 6%). There were isolated pixels with efficiencies as high as 97% and as low as 20%.

To correct for differential efficiency, the data for ^{3}H-strychnine binding were registered with the data for ^{3}H-succinimidyl propionate binding, and the ^{3}H-strychnine specific activity was divided by the relative efficiency of ^{3}H-succinimidyl propionate binding, pixel by pixel. This procedure resulted in the correction for differential efficiency of specific activity values for ^{3}H-strychnine binding as illustrated for both unsmoothed and smoothed ^{3}H-strychnine binding site distributions in Figure 2, *G, H*.

Although correcting for differential efficiency in this region of the mouse CNS did not change the areas of maximum binding, it did alter the relationship of binding between areas. This method for correcting differential efficiency should be generally applicable for tritium-generated autoradiograms. If the ligand cannot be dissociated completely from the section, then adjacent sections can be used for labeling with ligand and ^{3}H-succinimidyl propionate.

The quantification of receptor density in specific anatomical nuclei is typically performed by determining receptor density within the boundaries of anatomical nuclei from one or several sections taken through the nucleus and not from sections taken through the full extent of the nucleus. Similarly, frequently the quantification does not include the entire nucleus on a single section, but rather the area of greatest density or the center of the nucleus. Both of these practices bias quantification to the density found in small regions through the nucleus; they do not take into consideration the density throughout the nucleus. These problems can be solved by looking at the 3-dimensional distributions of receptors through anatomical regions and by demarcating nuclear boundaries from the morphological features of the section used to generate the autoradiograms.

The 3-dimensional distribution of quench-corrected ^{3}H-strychnine binding sites can be determined when the above procedures are carried out using serial sections through a single mouse brain and the information from adjacent sections is registered. Both the registration and viewing can be greatly improved by first converting the data from solid display format to isodensity contours that circumscribe regions of equivalent binding density. This is best accomplished using the data that have been smoothed. Isodensity contours for ^{3}H-succinimidyl propionate binding are shown in Figure 3*A* and for ^{3}H-strychnine binding in Figure 3*C*. The isodensity contour localization of ^{3}H-strychnine binding sites in relation to the outer limits of the tissue section is shown in Figure 3*B*. The image was generated by registering the isodensity contours for ^{3}H-strychnine binding to display the distribution of binding with the outermost isodensity contour from the ^{3}H-succinimidyl propionate binding which outlines the tissue section.

The 3-dimensional distribution of quench corrected ^{3}H-strychnine binding sites in the mouse brain as seen from 13 different angles is shown in Figure 4. In all 3-dimensional images the z-axis has been expanded 3-fold and a hidden-line algorithm has been performed to aid in viewing. A very low level of binding, 40 fmol/mg, is shown in Figure 4*A*; areas lying within the displayed contours contained ^{3}H-strychnine binding sites, while areas not lying within the contours did not contain ^{3}H-strychnine binding sites. A moderate level of binding, 320 fmol/mg, is shown in Figure 4*B*, and a high level of binding, 560 fmol/mg is shown in Figure 4*C*.

The 3-dimensional, quench-corrected distribution of ^{3}H-

←

Figure 2. Digitized, color-coded, and further processed images of the autoradiograms shown in Figure 1. The digitized, color-coded optical density of the distribution of relative quench measured by the binding of ^{3}H-succinimidyl propionate is shown in *A*. The distribution of the specific activity of ^{3}H-succinimidyl propionate binding determined by background subtraction and conversion to specific activity using a step-wedge standard is shown in *B*; and the smoothed specific activity distribution accomplished using a nearest neighbor smoothing algorithm is shown in *C*. The middle row contains the same information on the distribution of glycine receptors measured by ^{3}H-strychnine binding. Thus, *D* is the distribution of glycine receptors in optical density, *E* is the distribution in specific activity, and *F* is the smoothed specific activity. The quench-corrected distribution of glycine receptor specific activity and smoothed specific activity is shown in *G* and *H*. Quench is corrected by registering and then dividing the information on receptor distribution with the information on quench distribution, pixel by pixel, and multiplying the result by a factor that corrects for minimum quench and the relative efficiency between ^{3}H-succinimidyl propionate binding and the step-wedge standards as described in the text. The color code contains 15 colors; maximum binding is displayed as red, followed by pink, orange, yellow, greens, blues, purples, and grays. The same color table relating color to value is used for images *A* and *D*, for images *B* and *C*, and for images *E–H*. We have attempted to maintain the same relationship between the different color tables and the relative magnitude of the data.

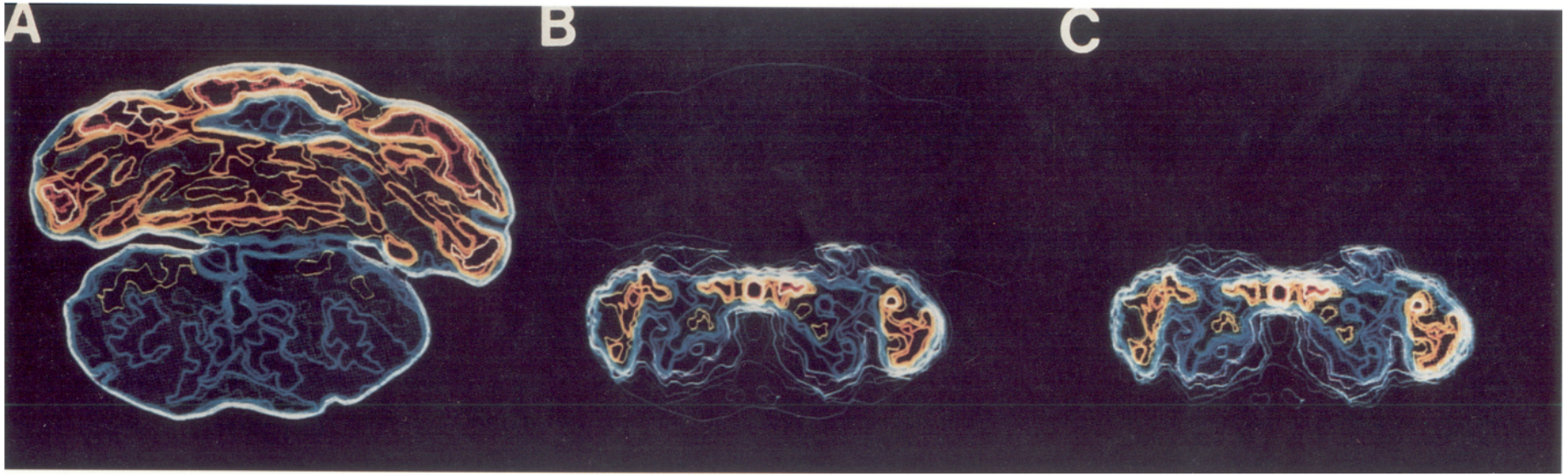

Figure 3. Isodensity contours of the distribution of the smoothed specific activity of relative quench (*A*) and quench-corrected glycine receptor specific activity (*C*) from the data shown in Figure 2, *C* and *H*. Isodensity contours of the different colors are drawn around areas of density equal to the lowest value found in that color category. All registration is performed using isodensity contours because they provide a transparent method for displaying the data. The lowest level isodensity contour (6% efficiency) for the binding of ^{3}H-succinimidyl propionate accurately defines the limits of the tissue section. The simultaneous display of this contour with the contours for the distribution of glycine receptors results in an image of the relative localization of the binding within the outline of the brain (*B*). These images are used for the display of the 3-dimensional distribution of binding.

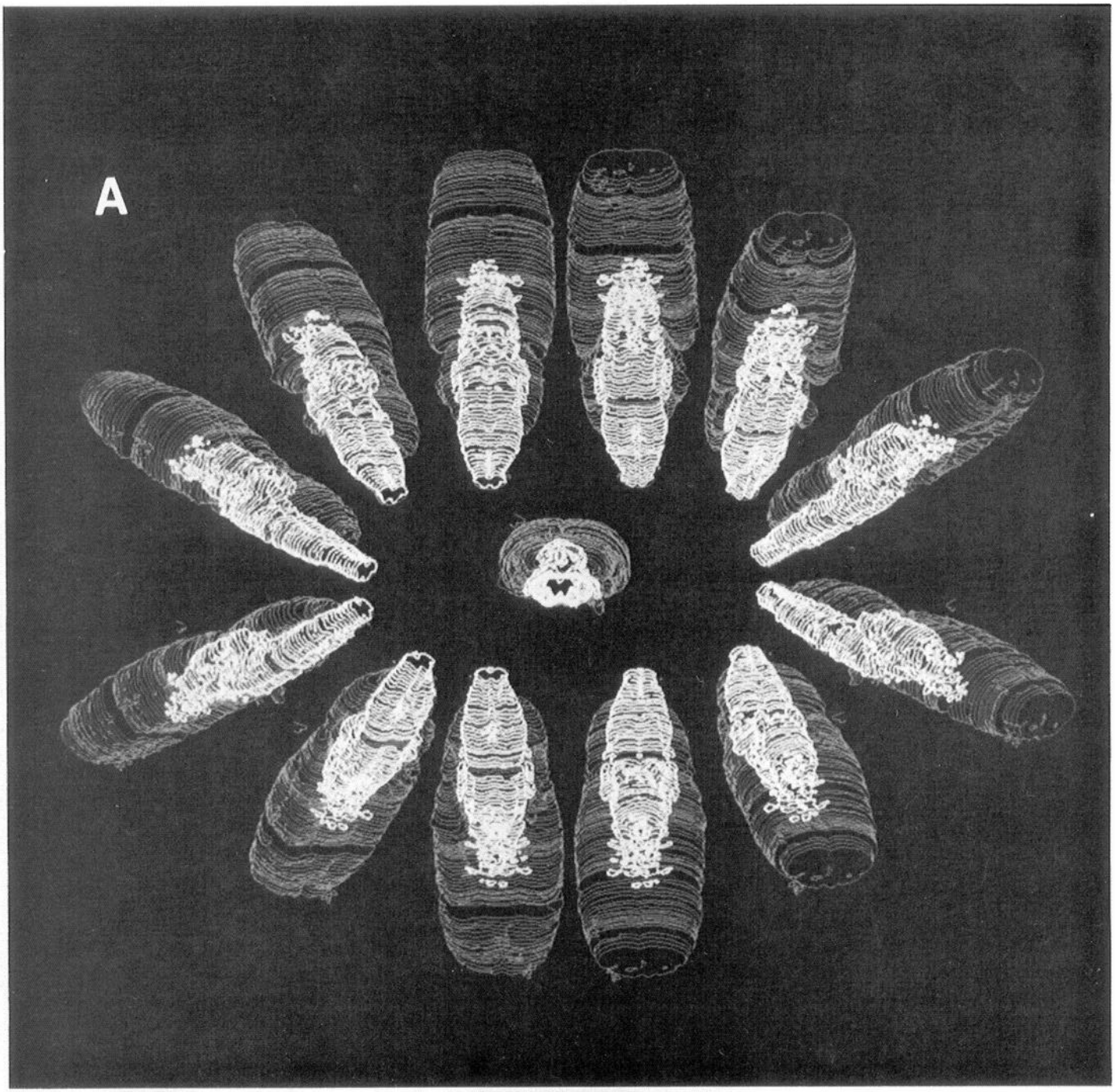

Figure 4. The 3-dimensional distribution of quench-corrected glycine receptor specific activity at a level of 40 fmol/mg (*A*), 320 fmol/mg (*B*), and 560 fmol/mg (*C*), viewed from 13 different angles. Isodensity contours of quench-corrected glycine receptor distribution and the lowest level of quench distribution to provide an outline of the brain from serial sections taken from C-3 to frontal pole were registered into 3-dimensional maps of receptor distribution. The sections were separated by an average of 120 μm; in all 3-dimensional images the z-axis has been expanded 3 times to facilitate viewing. The outlines of the sections are shown in gray; the isodensity contours for glycine receptor distribution are shown in white.

strychnine binding sites seen from a dorsal posterior viewing angle is shown in Figure 5*A*; each successive image is the 3-dimensional distribution of ^{3}H-strychnine binding sites at 40 fmol/mg higher levels of binding. Thus, the first image is the outline of areas containing greater than 40 fmol/mg, the second image is the outline for greater than 80 fmol/mg, and the last is the outline of binding greater than 600 fmol/mg. Figure 5*B* is the distribution of ^{3}H-strychnine binding sites viewed from a ventral anterior vantage. Fifteen levels of binding are shown ranging from greater than 40 to greater than 600 fmol/mg.

The receptor distribution information can also be registered with information on the boundaries of anatomical features of the tissue section as shown for the section illustrated in Figures 1–3 in Figure 6. It is then possible to extract the binding data based on anatomical location in a 3-dimensional fashion. This is done by determining the average density for the anatomical

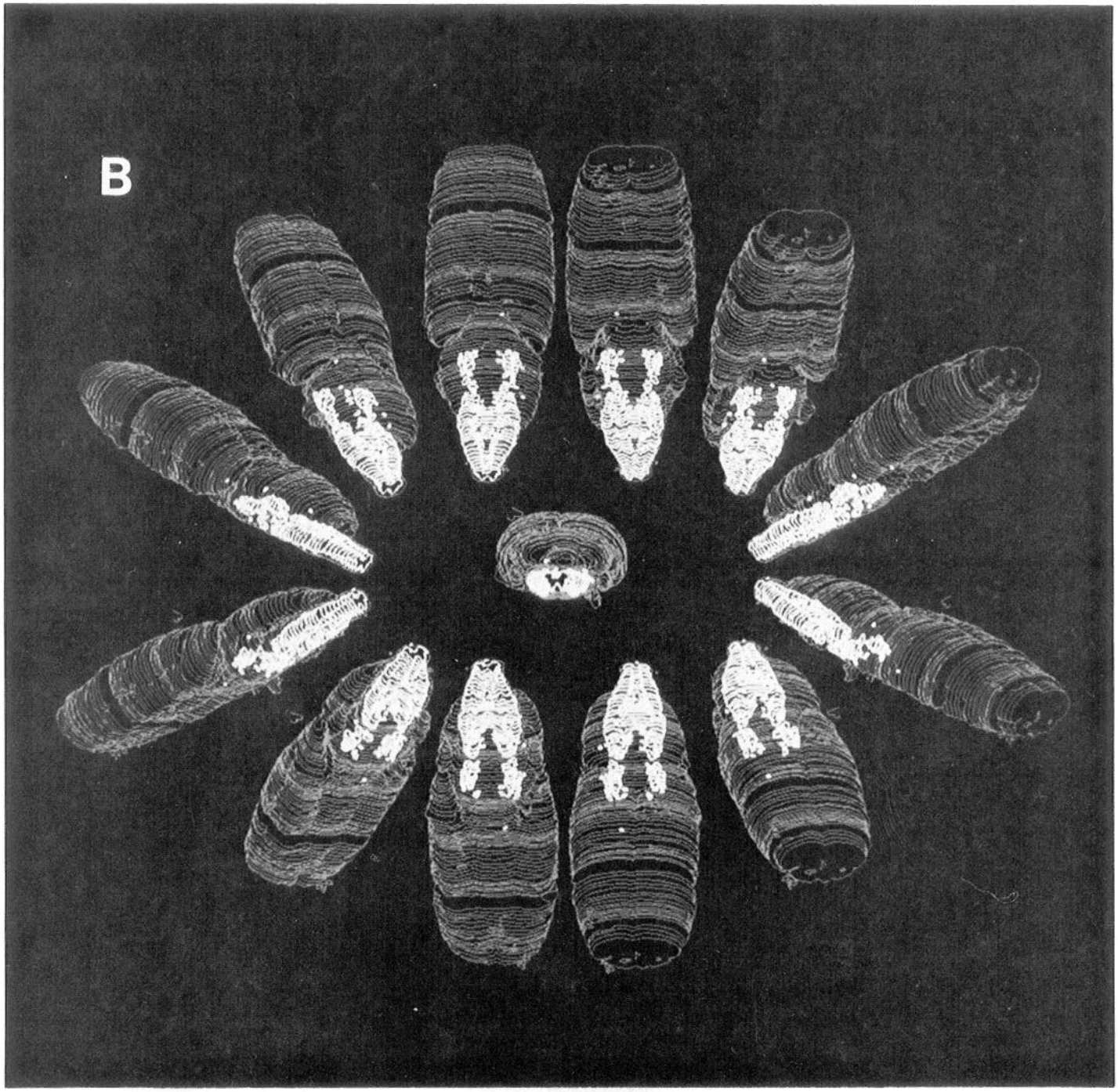

Figure 4. Continued

regions of interest for all the sections on which the regions are present. Values determined in this fashion for the 3-dimensional distribution of quench-corrected ^{3}H-strychnine binding sites in defined anatomical nuclei are shown in Table 1.

The value of analyzing receptor distribution data in this fashion is shown in Figures 7 and 8. Figure 7 illustrates the section-by-section binding of ^{3}H-strychnine to 3 nuclear groups: (*A*) the hypoglossal and prepositus hypoglossal nuclear group, (*B*) the substantia gelatinosa of the spinal cord and trigeminal nerve nuclear group, and (*C*) the medullary reticular formation nuclear group. The relative distribution of binding in each nuclear group was distinct, but the difference in binding seen between different sections illustrates an anterior-posterior heterogeneity in ^{3}H-strychnine binding. A similar heterogeneity for all the pixel values contained within nuclear boundaries is illustrated in Figure 8 for the (*A*) hypoglossal nucleus, (*B*) cuneate nucleus, and (*C*) ventral cochlear nucleus. From these examples it is apparent that it is important to sample as much of a nucleus as possible to determine the most accurate density of neurotransmitter receptor. Furthermore, these types of analyses make it possible to study the heterogeneity in terms of anatomical, functional, and other subdivisions within defined nuclei, as well as poten-

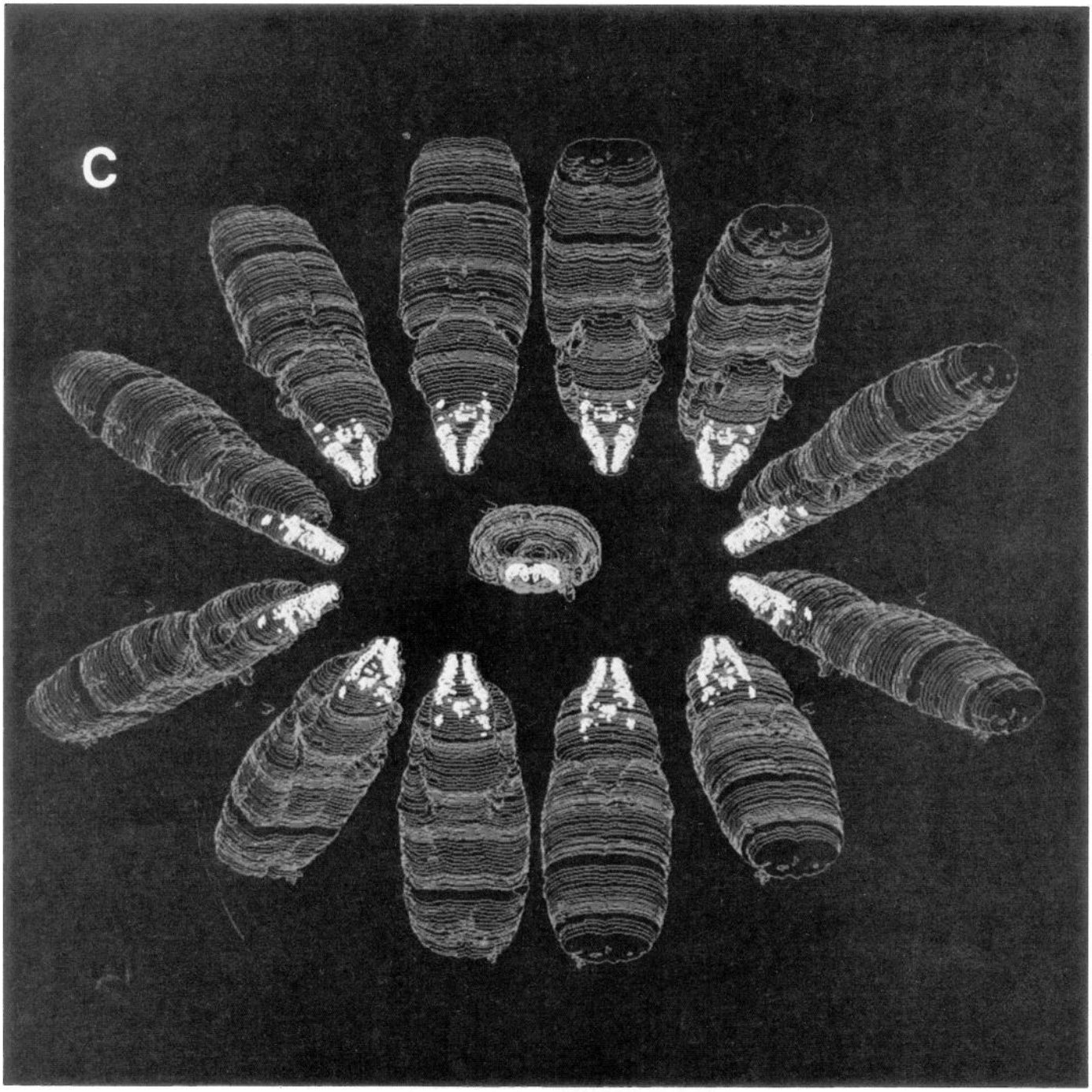

Figure 4. Continued

tially define other, as yet undefined subdivisions, biochemically. This information may provide insight into the parcellation of functional roles within nuclear subdivisions.

The highest levels of binding were seen in motor areas. Ventral layers of the spinal cord and the hypoglossal nucleus that innervate striated muscles had very high levels of ^{3}H-strychnine binding. Binding in Ro was about 30% that seen in 12. (See footnote to Table 1 for definitions of abbreviations.) Branchial efferent nuclei Amb, 7, P7, and Mo5 had moderate to high levels of binding; they contained very high levels of binding for nuclei at their more rostral locations. Nuclei involved in eye movements, 4, 6, and Dk had much lower binding than other motor areas. Moderate levels of binding were seen in autonomic motor area 10 and EW and AP had very low levels of binding. Binding in SNR of the extrapyramidal motor system was low to moderate but the highest of nuclei in the midbrain. There was a pronounced medial-ventral to dorsal-lateral gradient within SNR with more dorsal-lateral areas containing little binding; thus, medial-ventral areas within SNR have much higher binding than indicated by the mean. Binding in the SNC was about ⅓ that seen in SNR.

The substantia gelatinosa of the spinal cord and its rostral

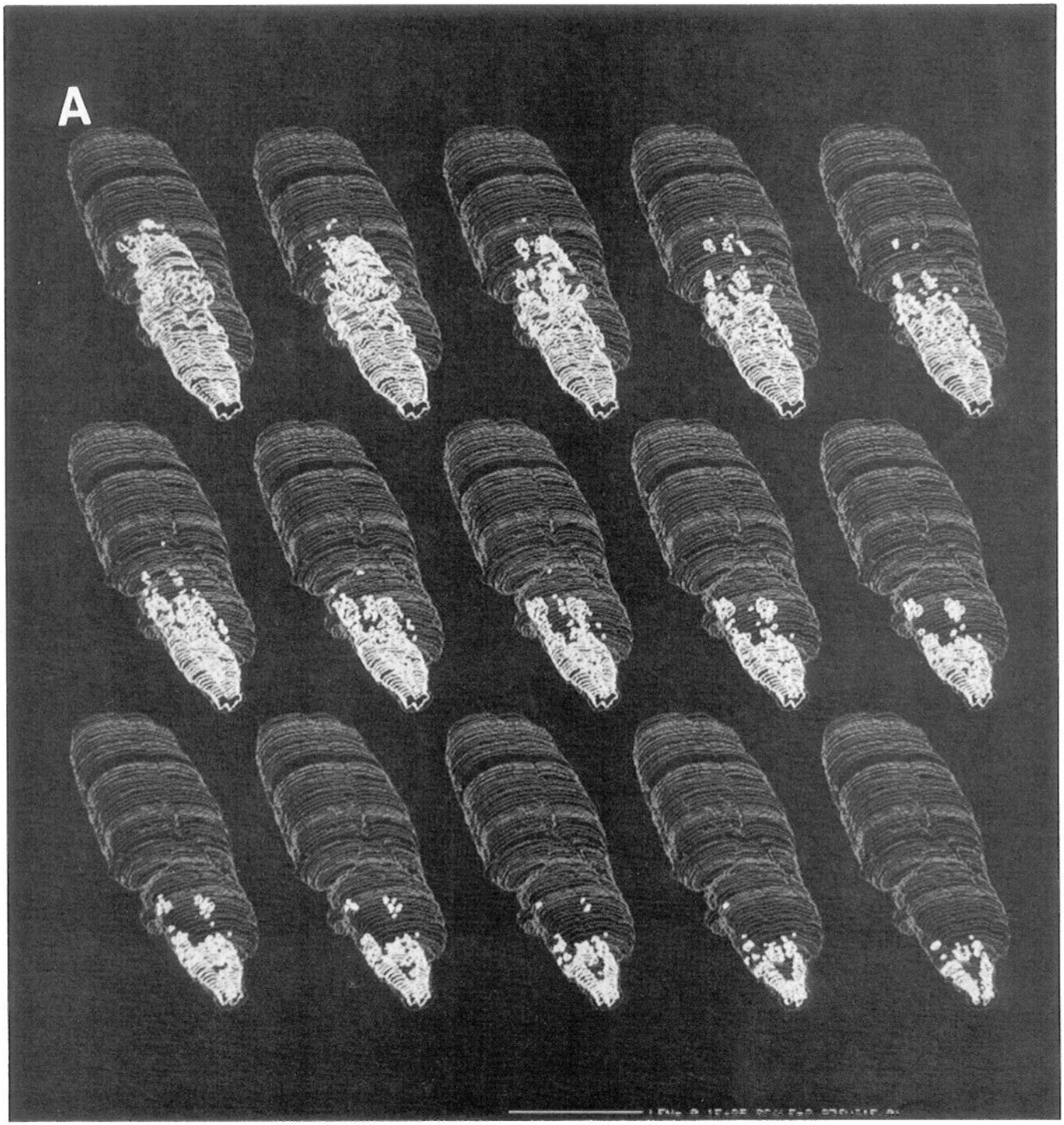

Figure 5. Three-dimensional distribution of quench-corrected glycine receptor specific activity from a dorsal posterior angle (*A*) and a ventral anterior angle (*B*). The data are similar to those shown in Figure 4 except that each figure shows the same angle but at 15 successively higher levels of binding, increasing by 40 fmol/mg tissue. The upper right image represents the distribution of binding greater than 40 fmol/mg, the next image the distribution greater than 80 fmol/mg, and so on; the bottom right represents binding greater than 600 fmol/mg.

extension into Sp5C, I, O, and Pr5 had very high levels of binding. There is a definite caudal-rostral gradient in this binding with cervical cord containing almost 3 times the number of binding sites as rostral sections of Sp5O and Pr5. Levels in Me5 were about ⅓ that seen in Sp5O and Pr5. Binding in the nuclei of the dorsal columns, Gr, and Cu was moderate, slightly higher than ½ that seen in the substantia gelatinosa at the same rostral-caudal levels; the associated GrC and ECu contained only about ⅓ the number of sites seen in Gr and Cu. The thalamic relay nuclei VPM and VPL contained no specific binding.

The nuclei of the special sensory afferents relaying auditory and vestibular information had lower binding than those involved in somatosensory function. Highest binding in the cochlear nuclei was found in DC, with about ⅔ as many sites in

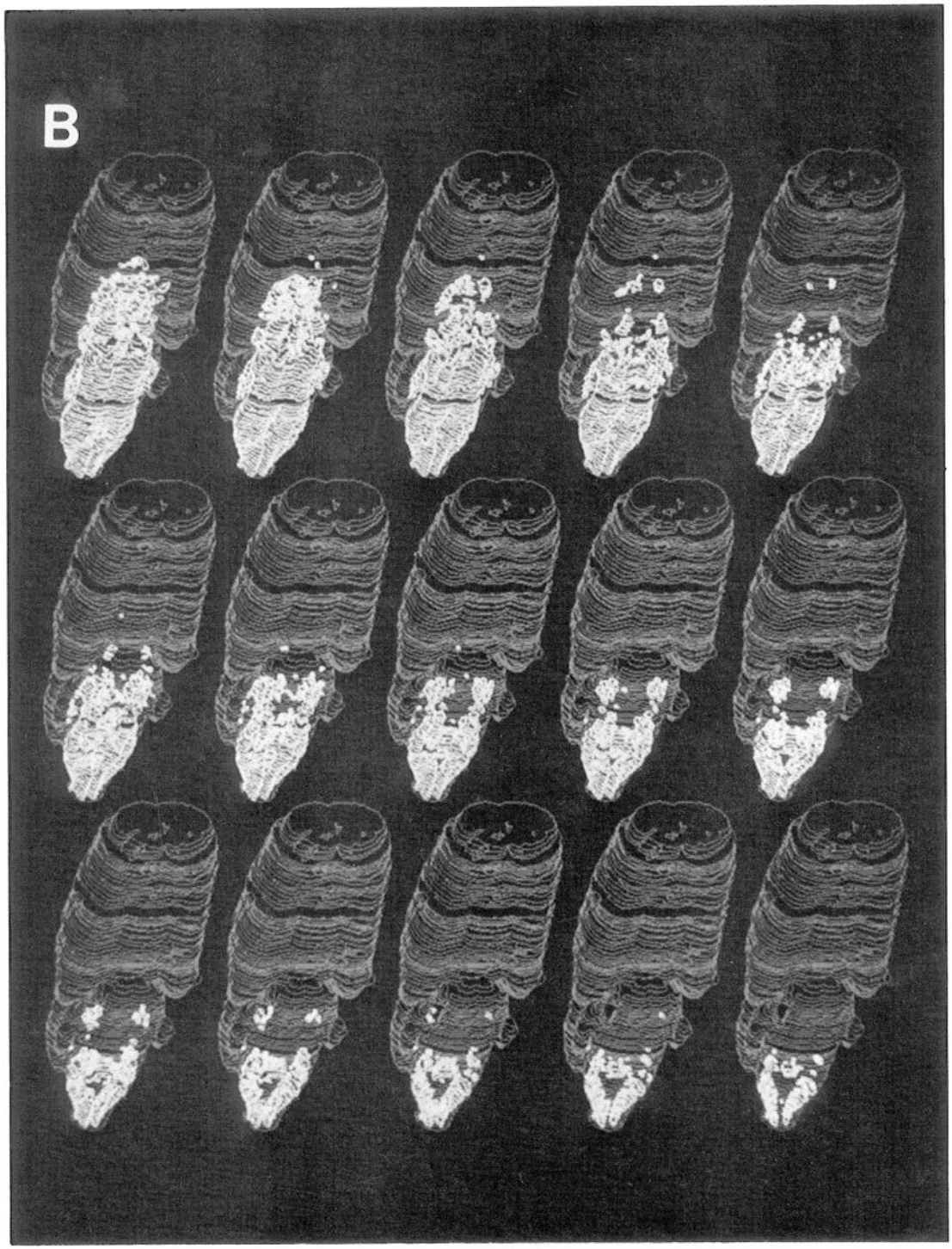

Figure 5. Continued

VC and ⅓ as many in VCP. In associated nuclei, the LSO had levels equivalent to DC, and the MSO had only about ½ the density of sites; the DLL and VLL were intermediate and TZ was much lower, with about 15% as many binding sites. The MVe was highest among the primary vestibular nuclei, being equal to the DC and LSO; SpVe had about ¾, LVe about ½, and SuVe about ¼ the number of binding sites. The CeC, which gives rise to spinovestibular projections, had almost 2½ times the density of sites as MVe. The associated PrH had about 30% more sites than MVe and X has about ½ the sites seen in MVe. The thalamic nuclei of the auditory system, MGD and MGV, had very low to no specific binding sites.

Binding in Sol, which receives autonomic afferents, had a moderate level of binding, comparable to that seen in MVe and DC; PSol had only about ½ the level of binding. Levels similar to PSol were seen in LPB and MPB and levels 50% greater than Sol in LPBI and 75% less are seen in the related PBG and KF.

The distribution of ^{3}H-strychnine binding sites in the reticular

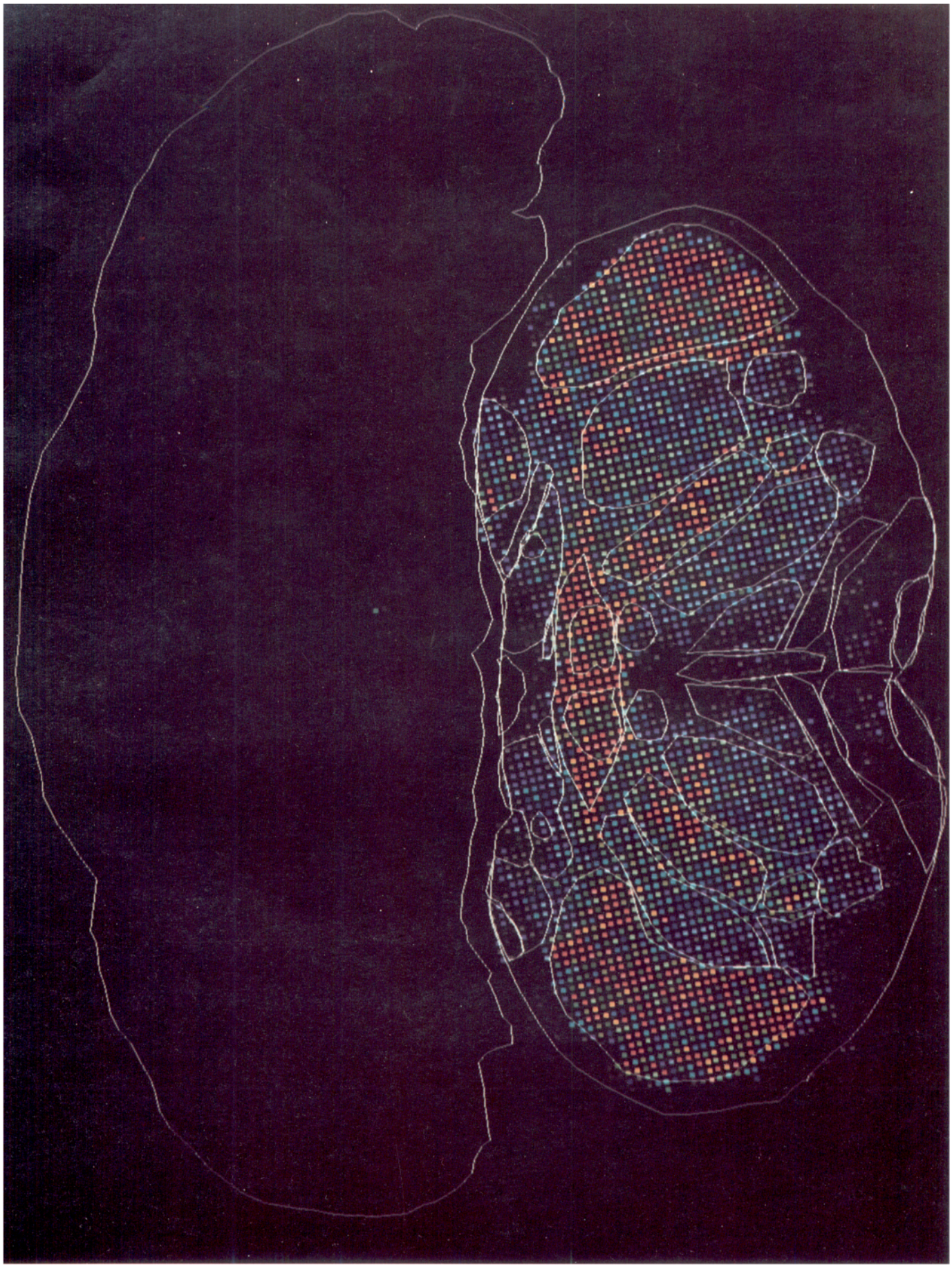

Figure 6. Superimposed images of the quench-corrected specific activity of ^{3}H-strychnine binding and boundary contours for anatomical nuclei drawn from the cresyl-violet-stained tissue section for the section shown in Figures 1–3. The nuclear boundary contours were used to define the specific activity values contained within anatomical regions.

Table 1. Three-dimensional, quench-corrected ^{3}H-strychnine binding specific activity in anatomical regions of the mouse brain

Area	Sections	Pixels	Mean	SD	Area	Sections	Pixels	Mean	SD
4	4	115	65	41	IO	9	1478	32	35
6	1	44	79	40	IP	3	521	11	15
7	4	901	318	119	IRt	11	2514	362	123
10	9	203	207	151	KF	2	105	65	55
12	8	948	558	184	L1	3	186	207	105
Amb	8	232	354	137	L23	3	464	670	246
Amyg	4	1441	32	30	L45	3	480	496	252
AP	4	203	19	18	L6	5	149	460	172
APT	10	3346	82	58	L7	7	595	520	173
Aq	12	1242	17	31	L89	8	1300	508	173
Arc	5	532	7	11	L10	8	207	349	161
bic	5	581	23	25	Lat	4	557	3	4
cc	3	9287	4	8	LC	10	573	92	51
CeC	7	143	491	141	LD	4	1255	5	15
CG	19	9652	73	44	LDTg	8	1195	107	56
CGPn	1	524	67	58	LH	4	860	36	36
CIC	7	1441	102	69	LHb	5	605	15	20
cic	2	417	41	33	Li	1	29	83	37
CL	2	227	13	17	ll	2	582	35	41
CM	2	132	9	15	LM	2	115	18	16
CnF	8	2338	56	36	LP	6	1024	11	20
cp	7	2854	4	13	LPB	6	781	112	89
Cu	12	1077	297	186	LPBI	1	64	331	204
cu	3	152	23	34	LPGi	6	722	168	93
DA	1	226	42	19	LRt	6	636	198	121
DCIC	6	2296	15	14	LRtS5	4	241	128	79
DC	4	680	191	144	LSO	11	1635	209	131
Dk	6	290	81	42	LVe	5	1118	96	71
DLG	8	1582	1	5	mcp	12	2980	8	32
DLL	3	488	148	118	MD	2	1303	13	19
DM	5	671	23	16	MdD	11	2978	375	147
DpG	12	7100	66	39	MdV	6	2309	375	159
DPGi	6	1031	174	100	Me5	13	598	105	60
DpMe	4	1128	99	57	Med	4	700	2	3
DR	12	655	70	49	MGD	6	1257	10	17
DTg	5	485	58	51	MGV	4	658	6	16
ECIC	11	7085	26	29	MHb	1	328	9	18
ECu	6	278	102	78	mlf	7	263	29	26
EW	4	63	22	19	MM	6	3504	13	15
FF	2	403	35	20	MnR	6	313	15	15
fr	10	526	23	28	Mo5	8	2177	356	145
G	3	417	7	13	MP	2	304	3	11
Gi	11	3959	245	108	MPB	5	309	138	93
GiV	9	823	147	101	MSO	4	495	108	88
Gr	12	453	299	201	mt	7	261	11	12
GrC	1	38	127	90	MVe	8	1721	209	86
I5	4	445	169	91	n5	4	567	16	37
icp	3	756	8	20	n7	4	1648	18	34
IMLF	2	59	72	47	n8	2	213	14	18
InCo	4	561	72	38	Op	2	440	64	35
Int	6	1597	3	6	OT	2	139	32	40
opt	2	80	15	53	SGe	1	67	151	58
P5	6	461	257	108	SM	1	48	5	5
P7	1	182	427	123	SNC	9	504	44	50
PBG	2	208	41	27	SNR	9	3169	127	135
PB	2	217	23	20	Sol	15	1597	206	117
PC	3	137	25	33	sol	2	14	131	87
pc	4	534	9	14	sp5	2	593	40	76
PCRt	12	3715	270	120	Sp5C	11	5789	568	224

Table 1. Continued

Area	Sections	Pixels	Mean	SD	Area	Sections	Pixels	Mean	SD
PF	4	2151	94	116	Sp5I	7	4039	439	199
PH	2	927	41	28	Sp5O	4	1526	288	131
PMn	4	633	150	93	SpVe	6	1461	156	84
PMR	4	266	20	21	STh	6	407	22	41
Pn	6	1918	17	26	Su5	3	219	225	72
PnC	3	1708	152	66	SubCA	1	45	82	48
PnO	11	6812	202	98	SubCD	8	811	144	72
PnV	2	280	143	62	SubCV	8	606	145	75
Po	11	4237	18	35	SuG	10	5892	84	64
PP	8	1054	27	35	SuM	2	40	15	10
Pr5	9	3420	302	184	SuVe	3	565	48	43
PrH	8	748	271	187	Tz	4	796	32	44
PSol	2	65	104	81	v3	4	36	6	9
PV	2	113	27	25	v4	4	245	39	48
py	12	1084	17	32	VC	10	1815	137	112
Rc	1	147	4	5	VCP	1	201	67	54
R	2	642	23	26	VLG	6	572	3	9
RMC	2	211	34	24	VLL	7	1244	174	131
RMg	10	342	125	96	VM	5	1070	10	15
ROb	10	270	86	69	VMH	5	785	38	28
Ro	1	43	186	164	VPL	5	2312	3	7
RPa	11	262	37	41	VPM	4	1486	3	10
RPn	7	228	58	68	VTA	5	734	40	29
Rt	1	100	1	2	VTg	4	195	25	15
RtTg	12	2412	63	85	X	2	84	89	56
RVL	5	485	322	153	xscp	4	334	20	19
scp	8	622	44	43	ZI	10	2853	34	50

The anatomical boundaries of nuclei and fiber pathways were digitized from camera lucida drawings made from the tissue sections stained with cresyl violet after autoradiography. The digitized boundary contours were registered with the receptor distribution data and used to define pixels localized to specific anatomical areas. The number of sections in which the region is found, the total number of pixels in the region, the mean of the quench-corrected specific activity values in those pixels, and the standard deviation are presented.

Abbreviations are those used by Paxinos and Watson (1986): 4, trochlear nucleus; 6, abducens nucleus; 7, facial nucleus; 10, dorsal motor nucleus of the vagus; 12, hypoglossal nucleus; Amb, ambiguus nucleus; Amyg, amygdala; AP, area postrema; APT, anterior pretectal nucleus; Aq, aqueduct (Sylvius); Arc, arcuate nucleus; bic, brachium of the inferior colliculus; cc, central canal; CeC, central cervical nucleus; CG, central gray; CGPn, central gray of the pons; CIC, central nucleus of the inferior colliculus; cic, commissure of the inferior colliculus; CL, centrolateral thalamic nucleus; CM, central medial thalamic nucleus; CnF, cuneiform nucleus; cp, cerebral peduncle, basal part; Cu, cuneate nucleus; cu, cuneate fasciculus; DA, dorsal hypothalamic area; DC, dorsal cochlear nucleus; DCIC, dorsal cortex of the inferior colliculus; Dk, nucleus of Darkschewitsch; DLG, dorsal lateral geniculate nucleus; DLL, dorsal nucleus of the lateral lemniscus; DM, dorsomedial hypothalamic nucleus; DpG, deep gray layer of the superior colliculus; DPGi, dorsal paragigantocellular nucleus; DpMe, deep mesencephalic nucleus; DR, dorsal raphe nucleus; DTg, dorsal tegmental nucleus; ECIC, external cortex of the inferior colliculus; ECu, external cuneate nucleus; EW, Edinger-Westphal nucleus; FF, fields of Forel; fr, fasciculus retroflexus; G, gelatinosis thalamic nucleus; Gi, gigantocellular reticular nucleus; GiV, gigantocellular reticular nucleus, ventral part; Gr, gracile nucleus; GrC, granular layer of the cochlear nuclei; I5, intertrigeminal nucleus; icp, inferior cerebellar peduncle (restiform body); IMLF, interstitial nucleus of the medial longitudinal fasciculus; InCo, intercollicular nucleus; Int, interposed cerebellar nucleus; IO, inferior olive; IP, interpeduncular nucleus; IRt, intermediate reticular nucleus; KF, Kolliker-Fuse nucleus; L1, layer 1 of the spinal cord; L23, layer 2 and 3 of the spinal cord; L45, layer 4 and 5 of the spinal cord; L6, layer 6 of the spinal cord; L7, layer 7 of the spinal cord; L89, layer 8 and 9 of the spinal cord; L10, layer 10 of the spinal cord; Lat, lateral (dentate) cerebellar nucleus; LC, locus coeruleus; LD, laterodorsal thalamic nucleus; LDTg, laterodorsal tegmental nucleus; LH, lateral hypothalamic area; LHb, lateral habenular nucleus; Li, linear nucleus of the medulla; ll, lateral lemniscus; LM, lateral mammillary nucleus; LP, lateral posterior thalamic nucleus; LPB, lateral parabrachial nucleus; LPBI, lateral parabrachial nucleus, internal part; LPGi, lateral paragigantocellular nucleus; LRt, lateral reticular nucleus; LRtS5, lateral reticular nucleus, subtrigeminal part; LSO, lateral superior olive; LVe, lateral vestibular nucleus; mcp, middle cerebellar peduncle; MD, mediodorsal thalamic nucleus; MdD, medullary reticular nucleus, dorsal part; MdV, medullary reticular nucleus, ventral part; Me5, mesencephalic trigeminal nucleus; Med, medial (fastigual) cerebellar nucleus; MGD, medial geniculate nucleus, dorsal part; MGV, medial geniculate nucleus, ventral part; MHb, medial habenular nucleus; mlf, medial longitudinal fasciculus; MM, medial mammillary nucleus, medial part; MnR, median raphe; Mo5, motor trigeminal nucleus; MP, medial mammillary nucleus, posterior part; MPB, medial parabrachial nucleus; MSO, medial superior olive; mt, mammillothalamic tract; MVe, medial vestibular nucleus; n5, trigeminal nerve; n7, facial nerve; n8, vestibulocochlear nerve; Op, optic nerve layer of the superior colliculus; OT, nucleus of the optic tract; opt, optic tract; P5, peritrigeminal zone; P7, perifacial zone; PB, parabrachial nuclei; PBG, parabigeminal nucleus; PC, paracentral thalamic nucleus; pc, posterior commissure; PCRt, parvocellular reticular nucleus; PF, parafascicular thalamic nucleus; PH, posterior hypothalamic area; PMn, paramedian reticular nucleus; PMR, paramedian raphe nucleus; Pn, pontine nuclei; PnC, pontine reticular nucleus, caudal part; PnO, pontine reticular nucleus, oral part; PnV, pontine reticular nucleus, ventral part; Po, posterior thalamic nuclear group; PP, peripeduncular nucleus; Pr5, principal sensory trigeminal nucleus; PrH, prepositus hypoglossal nucleus; PSol, parasolitary nucleus; PV, paraventricular thalamic nucleus; py, pyramidal tract; R, red nucleus; Re, reuniens thalamic nucleus; RMC, red nucleus, magnocellular part; RMg, raphe magnus nucleus; Ro, nucleus of Roller; ROb, raphe obscurus nucleus; RPa, raphe pallidus (postpyramidal raphe) nucleus; RPn, raphe pontis nucleus; Rt, reticular thalamic nucleus; RtTg, reticulotegmental nucleus of the pons; RVL, rostroventrolateral reticular nucleus; scp, superior cerebellar peduncle; SGe, supragenial nucleus; SM, nucleus of the stria medullaris; SNC, substantia nigra, compact part; SNR, substantia nigra, reticular part; Sol, nucleus of the solitary tract; sol, solitary tract; sp5, spinal trigeminal tract; Sp5C, spinal trigeminal nucleus, caudal part; Sp5I, spinal trigeminal nucleus, interpolar part; Sp5O, spinal trigeminal nucleus, oral part; SpVe, spinal vestibular nucleus; STh, subthalamic nucleus; Su5, supratrigeminal nucleus; SubCA, subcoerulus nucleus, alpha part; SubCD, subcoerulus nucleus, dorsal part; SubCV, subcoerulus nucleus, ventral part; SuG, superficial gray layer of the superior colliculus; SuM, supramammillary nucleus; SuVe, superior vestibular nucleus; Tz, nucleus of the trapezoid body; v3, third ventricle; v4, fourth ventricle; VC, ventral cochlear nucleus; VCP, ventral cochlear nucleus, posterior part; VLG, ventral lateral geniculate nucleus; VLL, ventral nucleus of the lateral lemniscus; VM, ventromedial thalamic nucleus; VMH, ventromedial hypothalamic nucleus; VPL, ventral posterolateral thalamic nucleus; VPM, ventral posteromedial thalamic nucleus; VTA, ventral tegmental area; VTg, ventral tegmental nucleus; X, nucleus X; xscp, decussation of the superior cerebellar peduncle; ZI, zona incerta.

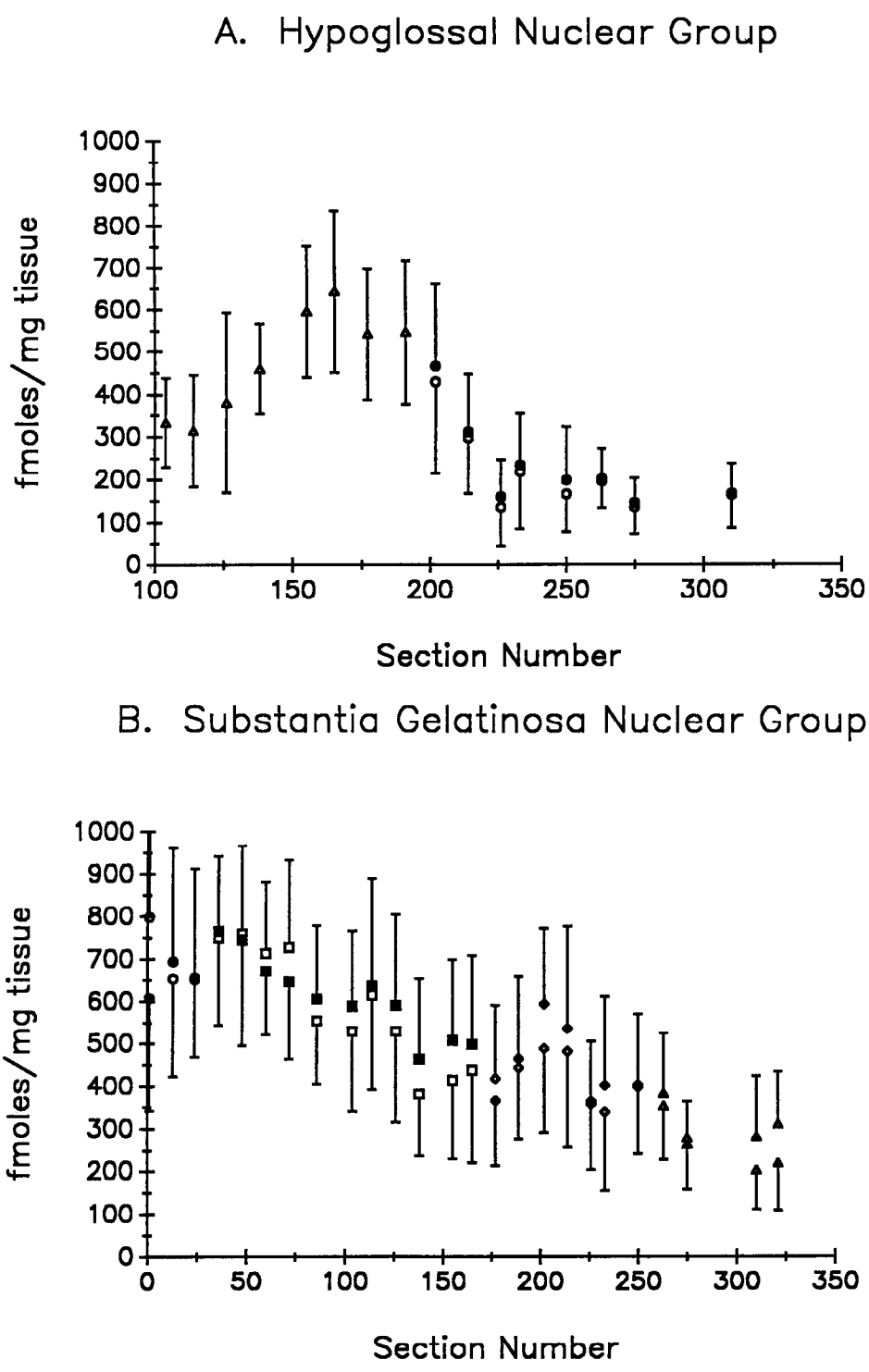

Figure 7. Quench-corrected specific activity of ^{3}H-strychnine binding to each section containing (*A*) 12 (▲) and PrH (●), (*B*) L2,3 (●), Sp5C (■), Sp5I (◆), and Sp5O (▲), and (*C*) MdD (●), MdV (▲), PCRt (▼), IRt (■), Gi (◆), LPGi (●), and GiV (■). Values are the mean ±SD; *open symbols* are values for the left side, *filled symbols* are values for the right side. The value determined for an area may vary considerably from section to section, and the SD for the value of an area determined on a single section is typically large. Both of these features indicate considerable variability in ^{3}H-strychnine binding density within a nucleus. These variations may show regional trends or may appear random.

formation generally followed the overall caudorostral distribution seen throughout the CNS, with more caudal regions having greater densities of sites than more rostral regions. Also, nuclei more centrally localized within the reticular core tended to have greater binding than nuclei situated more peripherally. Both MdD and MdV have comparable binding density, about ¾ the density in the adjacent Sp5C. More rostrally IRt maintains about the same density and both PCRT and Gi have about ¼ less binding. The medially located PMn, ventrally located GiV, and dorsally located DPGi all had less than ½ the density seen in IRt. This level of binding was comparable to that observed in PnC and PnV and about 30% less than that of PnO. The

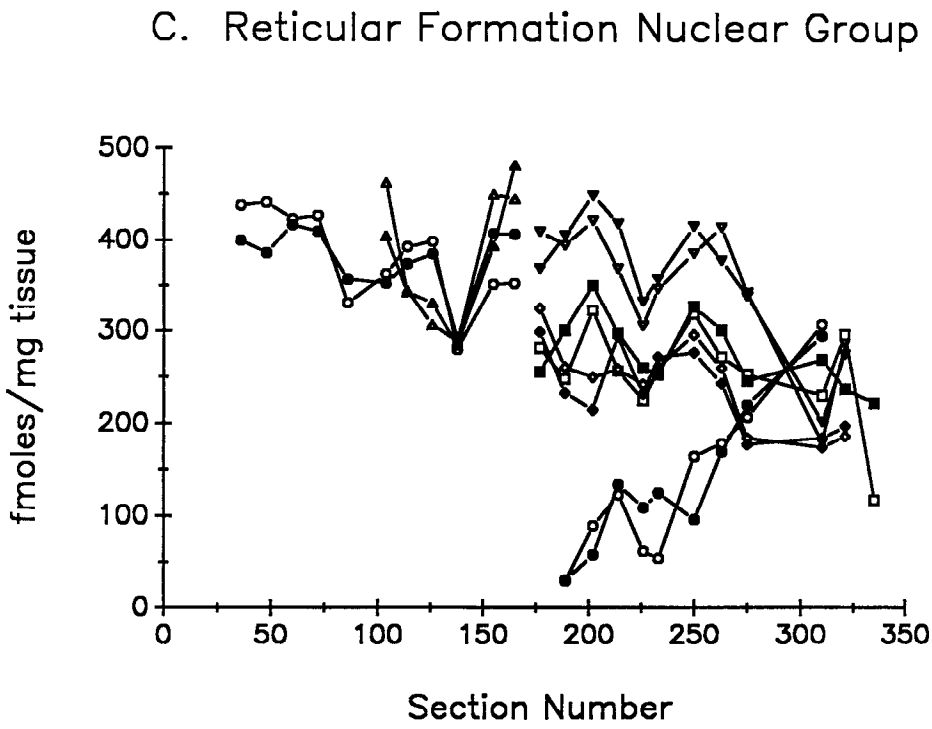

Figure 7. Continued.

CGPn and CG had about ½ the density of PnC and PnO; other surrounding nuclei including the tegmental nuclei, CNF, and DpMe had levels of binding generally similar to that of CG.

Binding within nuclei giving rise to diffuse projection systems, the raphe complex and LC, was generally low. Highest binding was in RMg, with a continuum of lower binding values in LC, ROb, DR, RPn, RPa, PMR, MnR, and finally IP, with less than 10% the binding seen in RMg.

The highest binding in the corpus quadrigemini was in CIC, with levels comparable to those of MSO and LVE. This level is only moderate for the rostrocaudal level of the colliculi. Much lower levels of binding were seen in ECIC, 25%, and DCIC, 15%. In the superior colliculus, SuG had the highest levels of binding, about 80% of CIC, and DpG and OP each had about 60% of the levels seen in CIC.

Neither the cerebellar cortex, nor the deep cerebellar nuclei Med, Int, or Lat had ^{3}H-strychnine binding above background. However, the precerebellar nuclei LRt and LPGi had moderate levels of binding, RtTg had about 70% fewer sites, IO and RMC had about 85% fewer sites, and R and Pn about 90% fewer sites.

Limbic areas had very low levels of binding. The VTA had the highest levels, but even this was very low. Levels barely above background were seen in LHb, MHb, and SM. Of some significance however, is the binding in the amygdala, which was the only telencephalic structure with specific binding.

Diencephalic nuclei had very low levels of binding. Comparable very low levels were seen in VMH, LH, DA, and PH. About ½ these values were found in LM, MM, SuM, and DM, and essentially background levels were seen in MP and Arc. In general, binding to thalamic nuclei was comparable to or even lower than that seen in the hypothalamus. The sole exception is PF, which bound 2½ times as much as the highest hypothalamic nucleus and 4 times the next highest thalamic nucleus. Binding in PF was highly specific to this nucleus and characteristically outlines fr. Nuclei with 4-5 times less binding include Po, STh, PC, and PV. It would be difficult to define other thalamic nuclei with binding significantly above background.

White-matter areas had binding densities equal to or barely above background. In general, in white-matter areas with binding above background, the binding could be attributed to areas immediately adjacent to surrounding gray matter. This was the case in spite of the relatively greater increase in specific activity due to the greater quench correction factors applied to white-matter areas.

Discussion

The results presented in this paper define the quench-corrected 3-dimensional distribution of ^{3}H-strychnine binding sites in the mouse CNS. Three-dimensional imaging techniques have been applied by others to autoradiographic data on the CNS (Hibbard and Hawkins, 1984; Stein et al., 1984; Davis et al., 1986). The methods presented here for determining the quench-corrected 3-dimensional distribution of neurotransmitter receptors enable accurate quantification of autoradiographic data on the distribution of not only neurotransmitter receptors, but also other features that can be autoradiographically localized. These data do not invalidate the work being performed by the numerous investigators applying receptor autoradiography to questions concerning chemical organization, but rather point the way to potential increased usefulness of the technique.

The biochemical (Graham et al., 1981, 1983; Pfeiffer and Betz, 1981; Pfeiffer et al., 1982) and pharmacological (Young and Snyder, 1973, 1974a, b; Mackerer et al., 1977) characteristics and regional distribution of ^{3}H-strychnine binding (Young and Snyder, 1973; Zarbin et al., 1981) indicate that this binding measures inhibitory postsynaptic glycine receptors. Strychnine does not label the recently described glycine binding site found in rostral brain areas (Bristow et al., 1986), which may be an allosteric site on the postsynaptic NMDA class of glutamate receptors (Johnson and Ascher, 1987).

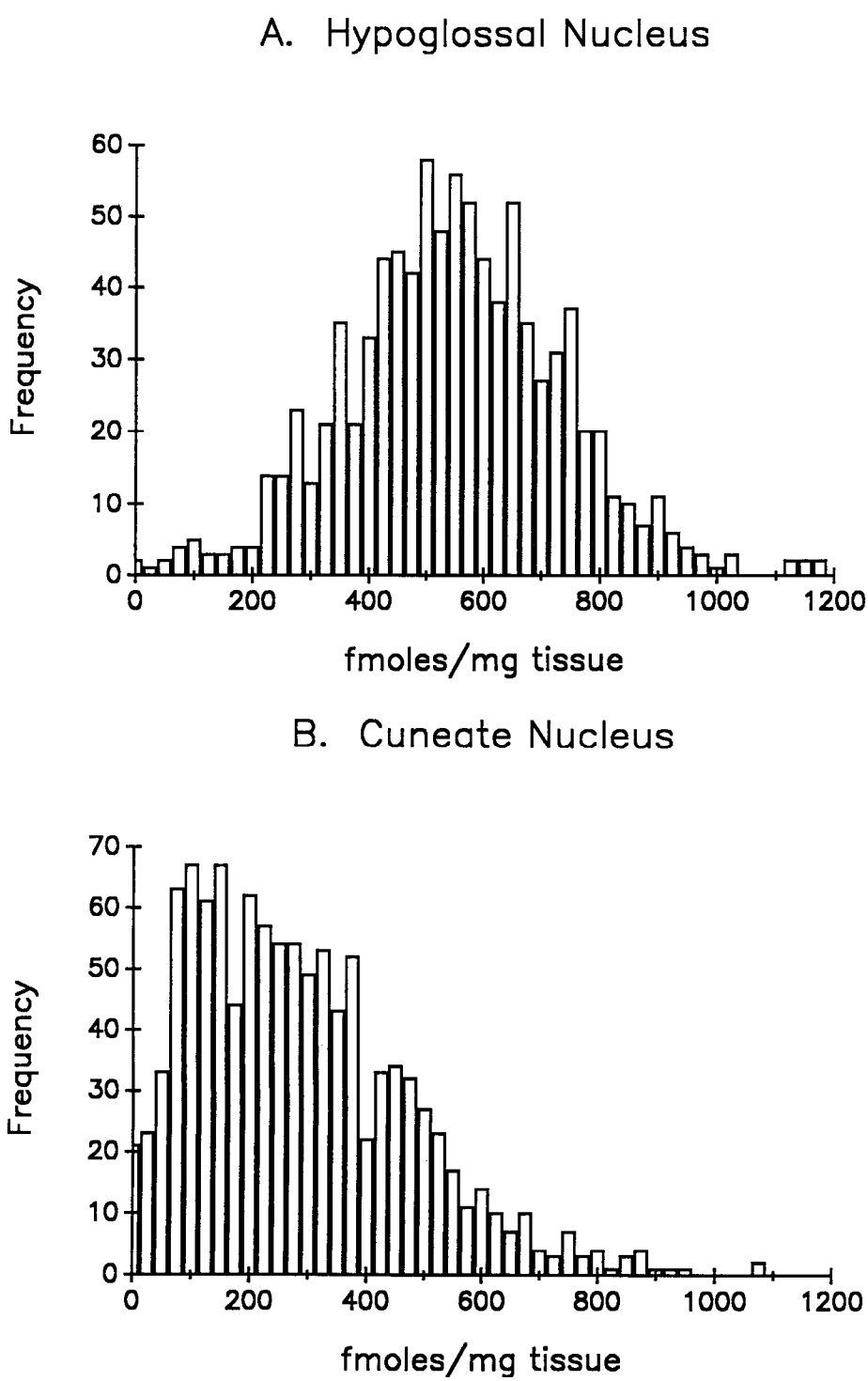

Figure 8. Histograms of quench-corrected ^{3}H-strychnine specific activity pixel values for (*A*) 12, (*B*) Cu, and (*C*) VC. The overall distribution of binding values may appear normal, as in *A* (even though the values for individual sections may show a trend—see Fig. 7), or be skewed, as in *B* and *C*. The relatively high number of 0 values seen in *C* and to a lesser extent *B* probably results from the incoming cochlear nerve and cuneate fasciculus fibers.

There is a great deal of similarity in the distribution of ^{3}H-strychnine binding between the mouse (Frostholm and Rotter, 1985), rat (Zarbin et al., 1981), and human (Probst et al., 1986). The posterior-anterior gradient is equally strong and there is a very good agreement in the overall density of binding sites among different areas. Somatic motor and sensory areas have the highest density of binding and special motor and sensory areas have lower, but still high, densities. Visceral afferent and efferent nuclei contain moderate levels of binding. The majority of the reticular formation has high to moderate levels of binding, with some of the more peripheral reticular nuclei containing lower levels. The inferior and superior colliculi have low levels of binding. Densities in the diencephalon are generally very low, as are densities in the limbic areas. The finding of specific binding in the amygdala is unique among telencephalic structures. Likewise, no specific binding is seen in the cerebellum or white-matter areas of the CNS.

The distribution of ^{3}H-strychnine binding sites correlates well with both biochemical and electrophysiological data on the distribution of the inhibitory glycine neurotransmitter system. It also provides biochemical support for the role of glycine-mediated inhibition in local sensory and motor processing as well

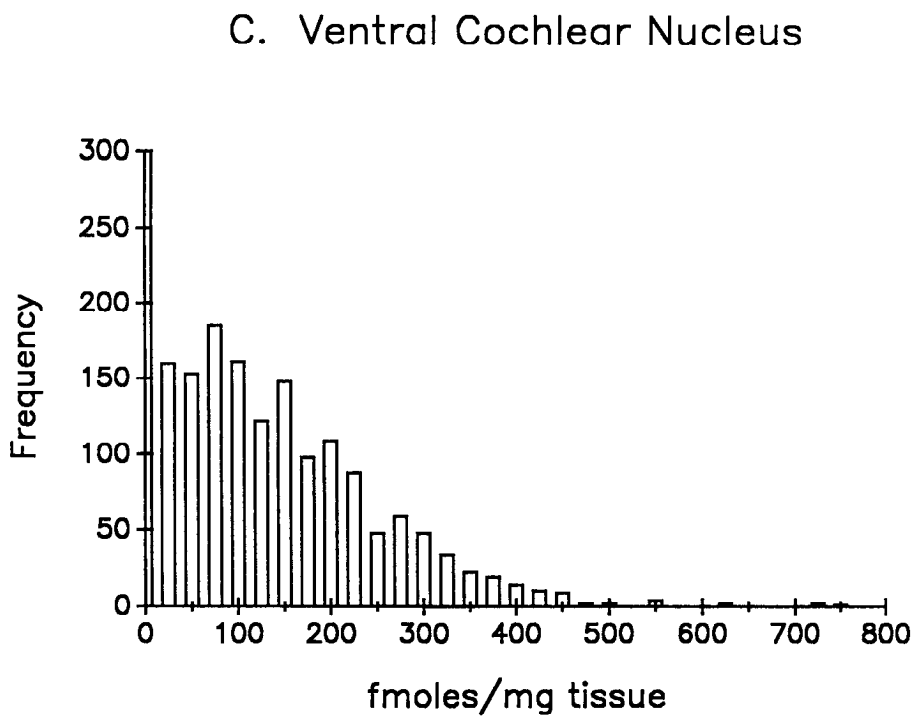

Figure 8. Continued.

as local integrative activities in the posterior CNS. Many of the functional implications of this distribution on a number of behaviors and strychnine toxicity have been discussed extensively (Zarbin et al., 1981). This discussion would be equally applicable to the mouse. The regional distribution of ^{3}H-strychnine binding sites and the functional implications of this distribution could explain the hyperexcitability, tremor, toe walking gait, and prolonged righting reflex seen in the spastic and spastic-Albany mutant mice, 2 allelic single-locus mutations in the mouse that have 80–95% fewer glycine receptors than controls (White and Heller, 1982; White, 1985; Becker et al., 1986; White et al., 1987). In addition, the distribution would predict abnormalities in audition and in visceral functions such as blood pressure and respiratory rate in these mutants.

The basic techniques presented in this paper, registration with other receptor binding data and tissue boundary contour data, and pixel-by-pixel mathematical functions enable pixel-by-pixel analysis and comparisons between data contained on adjacent sections. These data can be used to correct for differential efficiency as done in this study, to compare different neurotransmitter systems such as glycine and GABA receptors, or to compare different aspects of the same system such as different receptor subtypes, uptake sites versus receptor sites, and so forth.

In this paper we have looked at the heterogeneity in binding in the anterior-posterior dimension; a similar amount of heterogeneity would be expected in the dorsal-ventral, and medial-lateral planes. This analysis could be performed on the current database given the appropriate software. In many ways it would seem most appropriate to study heterogeneity in 3 dimensions simultaneously in order to determine distributions such as center weighted, peripheral, or patchy, all of which might be expected in neurotransmitter receptor localization material.

A number of technical questions are raised by the methods used in these studies. These questions relate to the optimal distance between serial sections used for the 3-dimensional reconstructions, the distance between isodensity contours in the 3-dimensional reconstructions, the amount of detail in the isodensity contours (i.e., the amount of smoothing), the similarity required between sections to permit intersection mathematical functions, the best way to adequately present the data, and many others. Although there are no definitive answers to any of these questions, the answer for any particular study must take into consideration the degree of anatomical resolution required by the specific questions being addressed, the section thickness, the resolution of the film, and the resolving power of the data acquisition instrument. Continued experimental experience with these variables will be required to define the optimal parameters.

One conclusion from this and numerous other studies on neurotransmitter receptor localization is that it is very difficult to present even a fraction of the data generated in such a study. It is impossible to distill the detailed localization information present in an autoradiographic image into a list of numbers that conveys the complexity of the underlying data. The use of techniques employed in this paper, such as correcting for differential efficiency and presenting data for the entire region on a series of sections taken through the rostrocaudal extent of the region, helps to present a more accurate representation of the data, but really is not useful for conveying the complexity. Some sense of complexity can be seen from the section-by-section data and the pixel histograms, but even here most of the anatomical information that may be very important for many types of analyses is lost. The only way to avoid these problems, and present an accurate representation of the complexity, is to present the actual data. However, there is so much data that this becomes difficult. Perhaps future developments in electronic data storage and management and its availability for publication purposes will permit the dissemination of this type of information. Certainly such a system would be a tremendous asset for the investigator interested in very detailed information on an area under study.

References

Alexander, G. M., R J. Schwartzman, R. D. Bell, J. Yu, and A. Renthall (1981) Quantitative measurement of local cerebral metabolic rate for glucose utilizing tritiated 2-deoxyglucose. Brain Res. *223:* 59–67.

Altar, C. A., R. J. Walter, K. A. Neve, and J. F. Marshall (1984) Computer-assisted video analysis of [^{3}H]spiroperidol binding autoradiographs. J. Neurosci. Meth. 10: 173–188.

Aprison, M. H., and N. S. Nadi (1977) Glycine: Inhibition from the sacrum to the medulla. In *Amino Acids as Chemical Transmitters,* F. Fonnum, ed., pp. 531–570, Plenum, New York.

Becker, C. M., I. Hermans-Borgmeyer, B. Schmitt, and H. Betz (1986) The glycine receptor deficiency of the mutant mouse spastic: Evidence for normal glycine receptor structure and localization. J. Neurosci. *6:* 1358–1364.

Bennett, J. P., and H. I. Yamamura (1985) Neurotransmitter, hormone, or drug receptor binding methods. In *Neurotransmitter Receptor Binding,* 2nd ed., H. I. Yammamura, S. J. Enna, and M. J. Kuhar, eds., pp. 61–89, Raven, New York.

Bristow, D. R., N. G. Bowery, and G. N. Woodruff (1986) Light microscopic autoradiographic localization of [^{3}H]glycine and [^{3}H]strychnine binding sites in rat brain. Eur. J. Pharmacol. *126:* 303–307.

Caviness, V. S., and D. S. Barkley (1971) Section thickness and grain count variation in tritium autoradiography. Stain Tech. *46:* 131–135.

Davis, D. W., A. M. Mans, J. F. Biebuyck, and R. A. Hawkins (1986) Regional brain glucose utilization in rats during etomidate anesthesia. Anesthesiology *64:* 751–757.

Falk, G. J., and R. D. King (1963) Radioautographic efficiency for tritium as a function of section thickness. Radiat. Res. *20:* 466–470.

Frostholm, A., and A. Rotter (1985) Glycine receptor distribution in mouse CNS: Autoradiographic localization of [^{3}H]strychnine binding sites. Brain Res. Bull. *15:* 473–486.

Geary, W. A., and G. F. Wooten (1985) Regional tritium quenching in quantitative autoradiography of the central nervous system. Brain Res. *336:* 334–336.

Geary, W. A., A. W. Toga, and G. F. Wootcn (1985) Quantitative film autoradiography for tritium: Methodological considerations. Brain Res. *337:* 99–108.

Goochee, C., W. Rasband, and L. Sokoloff (1980) Computerized densitometry and color coding of [^{14}C]deoxyglucose autoradiograms. Ann. Neurol. *73:* 359–370.

Graham, D., F. Pfeiffer, and H. Betz (1981) UV light-induced cross-linking of strychnine to the glycine receptor of rat spinal cord membranes. Biochem. Biophys. Res. Commun. *102:* 1330–1335.

Graham, D., F. Peiffer, and H. Betz (1983) Photoaffinity-labeling of the glycine receptor of the rat spinal cord. Eur. J. Biochem. *131:* 519–525.

Herkenham, M., and C. B. Pert (1982) Light microscopic localization of brain opiate receptors: A general autoradiographic method which preserves tissue quality. J. Neurosci. *2:* 1129–1149.

Herkenham, M., and L. Sokoloff (1984) Quantitative receptor autoradiography: Tissue defatting eliminates differential self-absorption of tritium radiation in gray and white matter of brain. Brain Res. *321:* 863–868.

Hibbard, L. S., and R. A. Hawkins (1984) Three-dimensional reconstruction of metabolic data from quantitative autoradiography of rat brain. Am. J. Physiol. *247:* E412–E419.

Johnson, J. W., and P. Ascher (1987) Glycine potentiates NMDA response in cultured mouse brain neurons. Nature *325:* 529–531.

Kuhar, M. J. (1985) Receptor localization with the microscope. In *Neurotransmitter Receptor Binding,* 2nd ed., H. I. Yamamura, S. J. Enna, and M. J. Kuhar, eds., pp. 153–176, Raven, New York.

Kuhar, M. J., and J. R. Unnerstall (1982) *In vitro* labeling receptor autoradiography: Loss of label during ethanol dehydration and preparative procedures. Brain Res. *244:* 178–181.

Kuhar, M. J., and J. R. Unnerstall (1985) Quantitative receptor mapping by autoradiography: Some current technical problems. Trends Neurosci. *8:* 49–53.

Kuhar, M. J., E. B. DeSouza, and J. Unnerstall (1986) Neurotransmitter receptor mapping by autoradiography and other methods. Annu. Rev. Neurosci. *9:* 27–59.

Mackerer, C. R., R. L. Kochman, T. F. Shen, and F. M. Hershenson (1977) The binding of strychnine and strychnine analogs to synaptic membranes of rat brainstem and spinal cord. J. Pharmacol. Exp. Ther. *201:* 326–331.

Palacios, J. M., D. L. Niehoff, and M. J. Kuhar (1981) Receptor autoradiography with tritium-sensitive film: Potential for computerized densitometry. Neurosci. Lett. *25:* 101–105.

Palacios, J. M., A. Probst, and R. Cortes (1986) Mapping receptors in the human brain. Trends Neurosci. *9:* 284–289.

Paxinos, G., and C. Watson (1986) *The Rat Brain in Stereotaxic Coordinates,* 2nd ed., Academic, New York.

Pfeiffer, F., and H. Betz (1981) Solubilization of the glycine receptor from rat spinal cord. Brain Res. *226:* 273–279.

Pfeiffer, F., D. Graham, and H. Betz (1982) Purification by affinity chromatography of the glycine receptor of rat spinal cord. J. Biol. Chem. *257:* 9389–9393.

Probst, A., R. Cortes, and J. M. Palacios (1986) The distribution of glycine receptors in the human brain. A light microscopic autoradiographic study using [^{3}H]strychnine. Neuroscience *17:* 11–35.

Rogers, A. W. (1979) *Techniques of Autoradiography,* Elsevier/North Holland, Amsterdam.

Sidman, R. L., J. B. Angevine, and E. Taber Pierce (1971) *Atlas of the Mouse Brain and Spinal Cord.* Harvard University Press, Cambridge, MA.

Stein, A., S. Juliano, P. Karp, and P. Hand (1984) Computer-assisted three-dimensional reconstructions of autoradiographic images of the cerebral cortex. J. Neurosci. Meth. *10:* 189–198.

White, W. F. (1985) The glycine receptor in the mutant mouse spastic (spa): Strychnine binding characteristics and pharmacology. Brain Res. *329:* 1–6.

White, W. F., and A. H. Heller (1982) Glycine receptor alteration in the mutant mouse spastic. Nature *298:* 655–657.

White, W. F., L. J. Regan, A. W. Roe, and A. Messer (1987) Behavior, genetics, and biochemistry of an allele of the mutant mouse spastic, spa^{Alb}. J. Neurogenet. *4:* 253–258.

Whitehouse, P. J. (1985) Receptor autoradiography: Applications in neuropathology. Trends Neurosci. *8:* 434–437. .

Young, A. B., and S. H. Snyder (1973) Strychnine binding associated with glycine receptors of the central nervous system. Proc. Natl. Acad. Sci. USA *70:* 2832–2836.

Young, A. B., and S. H. Snyder (1974a) Strychnine binding in rat spinal cord membranes associated with the synaptic glycine receptor: Cooperativity of glycine interactions. Mol. Pharmacol. *10:* 790–809.

Young, A. B., and S. H. Snyder (1974b) The glycine synaptic receptor: Evidence that strychnine binding is associated with the synaptic conductance mechanism. Proc. Natl. Acad. Sci. USA *71:* 4002–4005.

Young, W. S., III, and M. J. Kuhar (1979) A new method for receptor autoradiography: [^{3}H]opiod receptor labeling in slide mounted tissue sections. Brain Res. *179:* 255–270.

Zarbin, M. A., J. K. Wamsley, and M. J. Kuhar (1981) Glycine receptor: Light microscopic autoradiographic localization with [^{3}H]strychnine. J. Neurosci. *1:* 532–547.

Zilles, K., A. Schleicher, M. Rath, T. Glaser, and J. Traber (1986) Quantitative autoradiography of transmitter binding sites with an image analyzer. J. Neurosci. Meth. *18:* 207–220.